

Co-Delivery of Doxorubicin and Chloroquine by Polyglycerol Functionalized MoS₂ Nanosheets for Efficient Multidrug-Resistant Cancer Therapy

Shaohui Xu, Yinan Zhong, Chuanxiong Nie, Yuanwei Pan, Mohsen Adeli,* and Rainer Haag*

2D MoS₂ has shown a great potential in biomedical applications, due to its superior loading capacity, photothermal property, and biodegradation. In this work, polyglycerol functionalized MoS₂ nanosheets with photothermal and pH dual-stimuli responsive properties are used for the co-delivery of doxorubicin and chloroquine and treatment of multidrug-resistant HeLa (HeLa-R) cells. The polyglycerol functionalized MoS₂ nanosheets with 80 nm average size show a high biocompatibility and loading efficiency (≈90%) for both drugs. The release of drugs from the nanosheets at pH 5.5 is significantly promoted by laser irradiation leading to efficient destruction of incubated HeLa-R cells. In vitro evaluation shows that the designed nanoplatform has a high ability to kill HeLa-R cells. Confocal experiments demonstrate that the synthesized drug delivery system enhances the cellular uptake of DOX via folic acid targeting ligand. Taking advantage of the combined properties including biocompatibility and targeting ability as well as high loading capacity and photothermal release, this multifunctional nanosystem is a promising candidate for anticancer therapy.

malignant tumors.^[1–3] Autophagy is a possible mechanism for MDR, because it protects cancer cells against various stresses including starvation, hypoxia and anticancer drugs.^[4–6] Therefore, combining autophagy inhibitors and chemotherapeutic agents may pave the way for anti-MDR strategies. Chloroquine (CQ), which is employed as antimalarial drug clinically, is proved to be a chemosensitizer for cancer treatment in recent studies.^[7–10] It prevents the fusion of autophagosomes with lysosomes to form autolysosome. As a result, autophagosome degradation is disturbed over the later stages of autophagy.^[11,12] Hence a combination of CQ and anticancer drugs such as doxorubicin (DOX) can result in a synergistic effect in overcoming MDR.^[6,12–14]

2D nanomaterials including layered transition metal dichalcogenides (TMDCs) and black phosphorus have emerged as new vectors for a wide range of applications, owing to their extraordinary physical


and chemical properties.^[15,16] TMDCs (including MoS₂, MoSe₂, WS₂, and WSe₂) have shown outstanding performance in the field of sensors, catalysis, energy materials, drug delivery and photothermal therapy.^[15,17–20] In particular, MoS₂ nanosheets have demonstrated low toxicity and good biodegradability in vivo, which makes them potential candidates for biomedical applications.^[21,22] Nevertheless, the poor dispersibility and low stability of pristine MoS₂ in aqueous media hamper its bioapplications.^[23–25] These drawbacks can be surmounted by appropriate surface coating. Liu et al. have developed PEG functionalized MoS₂ nanosheets as a multifunctional nanocomposite for combined photothermal-chemo cancer therapy.^[23] They have found that the physiological stability and biocompatibility of MoS₂ significantly increased upon PEG functionalization. Hyperbranched polyglycerol (hPG) as a highly functional and water-soluble polymer has been used for the modification of 2D carbon nanomaterials.^[26–32] Modifying MoS₂ with hPG can improve its functionality, biocompatibility and water dispersibility. Wang et al have shown that modification of MoS₂ via physical adsorption of hPG improves the physicochemical properties of this material.^[33] However, noncovalent interactions between hPG and MoS₂ are not strong enough

1. Introduction

Multidrug resistance (MDR), which is defined as insensitivity or resistance of tumor cells to the encountered anticancer drugs, remains one of the greatest challenges in the chemotherapy of

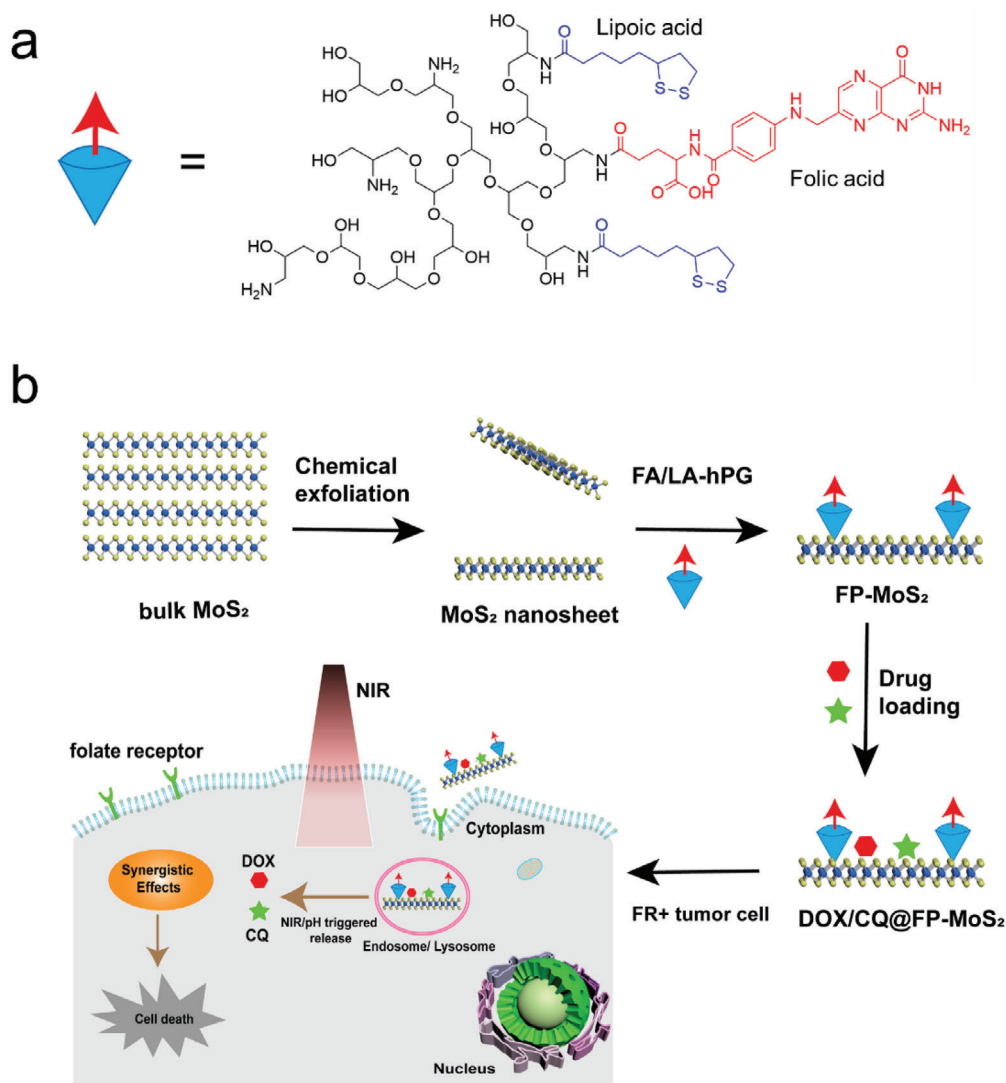
S. Xu, Y. Zhong, C. Nie, Y. Pan, R. Haag
 Institut für Chemie und Biochemie
 Freie Universität Berlin
 Takustr. 3, Berlin 14195, Germany
 E-mail: haag@zedat.fu-berlin.de

M. Adeli
 Faculty of Science
 Department of Chemistry
 Lorestan University
 Khorramabad Iran
 E-mail: adeli.m@lu.ac.ir

 The ORCID identification number(s) for the author(s) of this article can be found under <https://doi.org/10.1002/mabi.202100233>

© 2021 The Authors. Macromolecular Bioscience published by Wiley-VCH GmbH. This is an open access article under the terms of the Creative Commons Attribution-NonCommercial License, which permits use, distribution and reproduction in any medium, provided the original work is properly cited and is not used for commercial purposes.

DOI: 10.1002/mabi.202100233



Scheme 1. Schematic illustration of a) the chemical structure of folic acid and lipoic acid functionalized hPG (FA/LA-hPG) and b) the synthesis of FA/LA-hPG functionalized MoS₂ nanosheet (FP-MoS₂), loading of drugs on its surface and its applications for MDR cancer therapy (FR+ means folate receptor positive).

and may result in detachment of hPG from platform in blood circulation.

It is known that folate receptors are overexpressed on HeLa cells, opening a way to target nanomaterials to tumor sites by conjugation of folic acid (FA) to their surface. The active targeting and enhanced cellular uptake of the designed nanoplateforms by folic acid increase their therapeutic efficiency.^[34–38]

In this work, hPG was functionalized by FA and lipoic acid (LA) and then it was conjugated on MoS₂ nanosheets through disulfide linkages (Scheme 1a). Afterward, DOX and CQ were loaded onto the hPG-functionalized MoS₂ nanosheets for MDR cancer therapy (Scheme 1b). Release of drugs from hPG-functionalized MoS₂ nanosheets containing folic acid ligands (FP-MoS₂) at different conditions was also investigated. Moreover, the *in vitro* MDR effects of this targeted drug delivery system against human MDR cancer cell line (HeLa resistant cells) was studied.

2. Results and Discussion

In order to synthesize FA/LA-hPG, some of the hydroxyl functional groups of hPG were converted into amino groups and folic and lipoic acids were conjugated to this polymer by amide coupling. Reaction between sulfur atoms of MoS₂ nanosheets and lipoic acid tails of FA/LA-hPG resulted in FP-MoS₂ (Scheme 1). In the ¹H NMR spectrum of the modified hPG, signals at 1.4–2.4 ppm and 6.5–9 ppm are assigned to the lipoic acid and folic acid, respectively (Figure S1, Supporting Information). Peaks area ratios showed that 1% and 2% of hPG functional groups are conjugated to folic acid and lipoic acid, respectively.

The morphology and size of MoS₂ nanosheets was investigated by electron microscopies. The SEM image in Figure 1a showed relatively uniform sheet-like structures for the pristine MoS₂ nanosheets. In TEM analysis, a typical thin-layered nanostructure was observed, demonstrating that MoS₂ has

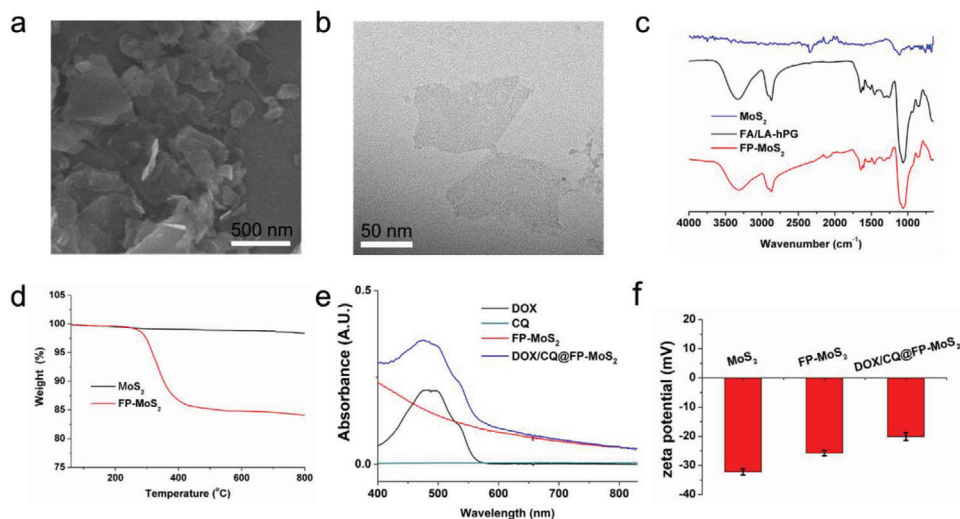


Figure 1. a,b) SEM and TEM images of the pristine MoS₂ nanosheets. c) IR spectra of pristine MoS₂ nanosheets, FA/LA-hPG and FP-MoS₂. d) TGA curves of pristine MoS₂ and FP-MoS₂ under argon. e) UV–vis absorbance spectra of free DOX (5 μg mL⁻¹), free CQ (5 μg mL⁻¹), FP-MoS₂ (40 μg mL⁻¹), and DOX/CQ@FP-MoS₂ (DOX and CQ at 5 μg mL⁻¹, and FP-MoS₂ at 40 μg mL⁻¹) in aqueous solutions. f) Zeta potential of MoS₂ nanosheets (40 μg mL⁻¹), FP-MoS₂ (40 μg mL⁻¹) and DOX/CQ@FP-MoS₂ (DOX and CQ at 5 μg mL⁻¹, and FP-MoS₂ at 40 μg mL⁻¹).

been exfoliated successfully (Figure 1b). The size distribution of pristine MoS₂ nanosheets and FA/LA-hPG (FP)- functionalized MoS₂ nanosheets (FP-MoS₂) were also obtained from TEM images. The pristine MoS₂ nanosheets showed an average lateral size of ≈100 nm (Figure S2, Supporting Information). After modification of MoS₂ nanosheets by hPG, the average diameter of FP-MoS₂ nanosheets decreased to around 80 nm, which is in a good regime for the body circulation. The reduction of the sheets size was due to the sonication process employed in the preparation of FP-MoS₂. Structure and functionality of the synthesized materials were further investigated by infrared spectrometry (IR). Absorbance bands at 1642 and 1561 cm⁻¹ were ascribed to the amide bonds, which attached folic acid and lipoic acid to the hPG, as well as C=C and C=N bonds in the folic acid structure. (Figure 1c). Absorbance bands at 3342, 2871, and 1066 cm⁻¹ that appeared at both FA/LA-hPG and FP-MoS₂ spectra were assigned to O–H, C–H, and C–O stretching vibrations of polyglycerol and conjugated ligands. TGA was also performed to obtain more information about the composition of the synthesized materials. The pristine MoS₂ showed a low weight loss (1.6 wt%) between 200 and 800 °C, which could be ascribed to the decomposition of residual organic materials such as n-BuLi (Figure 1d). However, FP-MoS₂ showed 17.1% weight loss at the same temperature range, which was assigned to the FA/LA-hPG component. Pristine MoS₂ nanosheets were soluble in water owing to their negative charge but they are prone to aggregation in the presence of inorganic salts, e.g. PBS. Therefore, they were not stable under physiological conditions. Accordingly, the stability of FP-MoS₂ under physiological conditions was investigated. As it can be seen from **Figure 2a,b**, the stability and dispersibility of MoS₂ nanosheet were remarkably improved after conjugation of FA/LA-hPG to their surface. An 1 mg mL⁻¹ solution of FP-MoS₂ in PBS and cell culture medium was stable for 7 days at 4 °C. UV–vis spectra of FP-MoS₂ did not show any significant change in absorption of this nanomaterial after functionalization

compared with pristine MoS₂ (Figure S3, Supporting Information). This result indicated the absorption properties of FP-MoS₂ in NIR region maintained after functionalization.

The effect of combination of free DOX and CQ against HeLa-R cells was evaluated.

Synergistic effects for all tested mass ratios were observed (Table S2). CI reached its minimal value when the mass ratio of DOX/CQ was 1:1. Therefore, we chose this mass ratio in the subsequent experiments.

In order to create a multifunctional drug delivery system, FP-MoS₂ was loaded by DOX and CQ molecules and DOX/CQ@FP-MoS₂, which was potentially suitable for photochemotherapy. The UV–vis spectrum of the DOX/CQ@FP-MoS₂ exhibited the absorption peaks of DOX at 490 nm, indicating the successful loading of this drug by FP-MoS₂ (Figure 1e). Furthermore, the surface charge of the pristine MoS₂ was changed from -32.2 mV to -25.8 mV and -20.1 mV after functionalization by FA/LA-hPG and DOX/CQ co-loading, respectively (Figure 1f). This is a further proof for the successful functionalization of MoS₂ nanosheets and loading by the drug cargos. Coating of MoS₂ nanosheets surface by FA/LA-hPG passivate their surface and decrease their negative surface charge. Also, loading of drugs further decreased the negative surface charge of FP-MoS₂ nanosheets due to the positive charges originated from amino functional groups of the loaded drugs.

MoS₂ nanosheets exhibit a high photothermal conversion efficiency, which is beneficial for photothermal therapy. The photothermal effect of FP-MoS₂ was investigated by measuring the temperature variations of the solutions under 808 nm NIR irradiation. As shown in Figure 2c, a concentration-dependent photothermal effect was observed for this material. The photothermal property of FP-MoS₂ was concentration-dependent and the temperature of medium increased by 45 °C after three minutes laser irradiation of a 200 μg mL⁻¹ aqueous solution. Figure 2d displays the laser-power-dependent photothermal

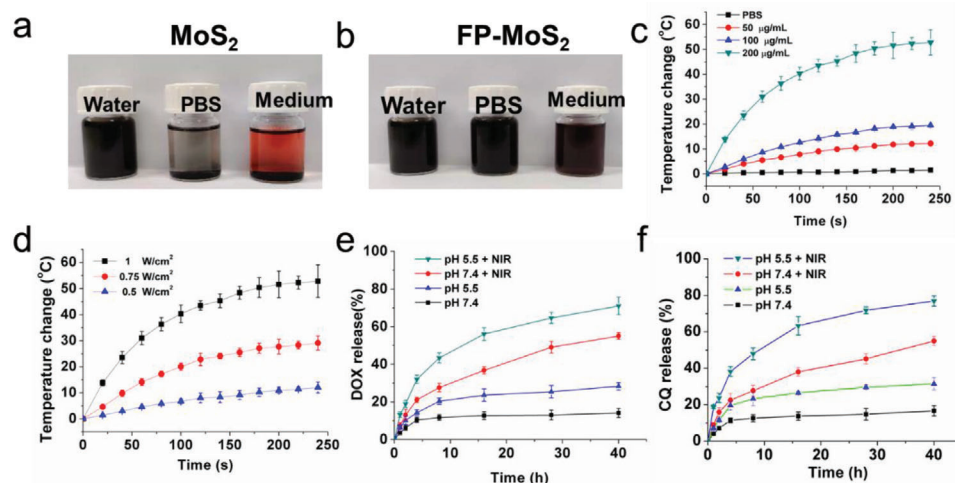


Figure 2. Photographs of a) MoS_2 (1 mg mL^{-1}) and b) FP- MoS_2 nanosheets (1 mg mL^{-1}) dispersed in Mill Q water, pH 7.4 PBS and DMEM cell culture medium (containing 10% serum) for 7 days at 4°C . c) Temperature change curves of the FP- MoS_2 solutions with different concentrations at a laser power density of 1 W cm^{-2} for 4 min. d) Temperature change curves of the FP- MoS_2 aqueous dispersion ($200 \mu\text{g mL}^{-1}$) at different laser power densities for 4 min. Release profile of e) DOX and f) CQ from DOX/CQ@FP- MoS_2 at pH 5.5 and pH 7.4 in PBS with and without NIR irradiation (1 W cm^{-2} for 4 min).

effect of the FP- MoS_2 ($200 \mu\text{g mL}^{-1}$) with different irradiation power densities. While 0.5 W cm^{-2} laser-power did not change the temperature of the medium significantly, a 1 W cm^{-2} laser irradiation induced a considerable temperature change after a few minutes. These results indicated that the functionalized FP- MoS_2 was able to convert laser irradiation to heat using a suitable laser power and thus is suitable for photothermal therapy.

The loading efficiencies of DOX and CQ by FP- MoS_2 were calculated to be 88.9 and 92.4 wt%, respectively. These high drug loading efficiencies which were due to the huge surface area and high negative charge of MoS_2 nanosheets implied the great potential of FP- MoS_2 as a drug carrier.

Release of loaded drugs from FP- MoS_2 was studied at different conditions. While 14.1% of DOX and 16.6% of CQ were released from DOX/CQ@FP- MoS_2 at pH 7.4 after 40 h, the release of these drugs raised to 28.3% (DOX) and 31.4% (CQ) at pH 5.5 (Figure 2e,f). The pH-dependent release of both DOX and CQ is favorable for tumor therapy, since the tumor environment and tumor cell endosomes are both acidic. The higher release of drugs at pH 5.5 was attributed to the enhanced protonation and hydrophilicity of drugs in acidic medium. Also laser irradiation triggered the release of DOX and CQ from the nanosheets. The increased drug release under NIR irradiation was assigned to the increased Brownian motion of drugs under local heating of MoS_2 nanosheets.

IC_{50} values of HeLa-R cells and HeLa cells are 14.19 and $0.86 \mu\text{g mL}^{-1}$, respectively, demonstrating a strong resistance of HeLa-R cells to DOX (Figure S4 and Table S1, Supporting Information). Therefore, HeLa-R cells were used as the drug resistance cancer cells in the following experiments.

Since biocompatibility is crucial for biomedical applications of nanomaterials, the toxicity of the synthesized materials against HeLa-R cells was investigated. The viability of cells that were incubated with FP- MoS_2 was much higher than those incubated with the pristine MoS_2 nanosheets. The viability of HeLa-R cells

decreased to 75.0% upon incubation with MoS_2 nanosheets ($160 \mu\text{g mL}^{-1}$) for 48 h, whereas more than 90% of these cells were not affected by FP- MoS_2 under the same conditions (Figure 3a). This result demonstrated that the functionalization of MoS_2 nanosheet by hPG improved its biocompatibility significantly.

Figure 3b shows the cytotoxicity of the FP- MoS_2 against HeLa-R cells at different concentrations with and without laser irradiation. The observed cytotoxicity under NIR irradiation at $80 \mu\text{g mL}^{-1}$ can be assigned to the photothermal effect. However, there was no significant difference in cell viability of cells treated with free DOX/CQ with and without NIR irradiation (Figure 3c).

The anticancer property of DOX/CQ@FP- MoS_2 was investigated and results are shown in Figure 3d. While some effects for the free drugs were observed, a synergistic anticancer effect was observed for their combination. Accordingly DOX and CQ were co-loaded on the surface of FP- MoS_2 for a synergistic chemotherapy as well as a photothermal effect. Interestingly, DOX/CQ@FP- MoS_2 under laser irradiation showed the highest anticancer activity, due to the above-mentioned properties and its efficient targeting drug delivery abilities. Only 18.3% of HeLa-R cells survived after 48 h incubation with DOX/CQ@FP- MoS_2 and 4 minutes laser irradiation.

A live/dead assay was carried out to further assess the *in vitro* antitumor effects of DOX/CQ@FP- MoS_2 . Calcein-AM and EthD-1 were used to double stain cells and to visualize live and dead cells. While no significant dead cell population was found in the control group, free DOX/CQ showed a low antitumor activity after 6 h incubation with HeLa-R cells (Figure 3e). DOX/CQ@FP- MoS_2 illustrated strong anticancer effect, which could be attributed to the folic acid targeting moiety leading to increased drug internalization in tumor cells. Upon NIR irradiation, the vast majority of cells were destroyed, suggesting that the chemo-photothermal therapy by DOX/CQ@FP- MoS_2 has an outstanding anti-MDR efficiency and is of high potential for

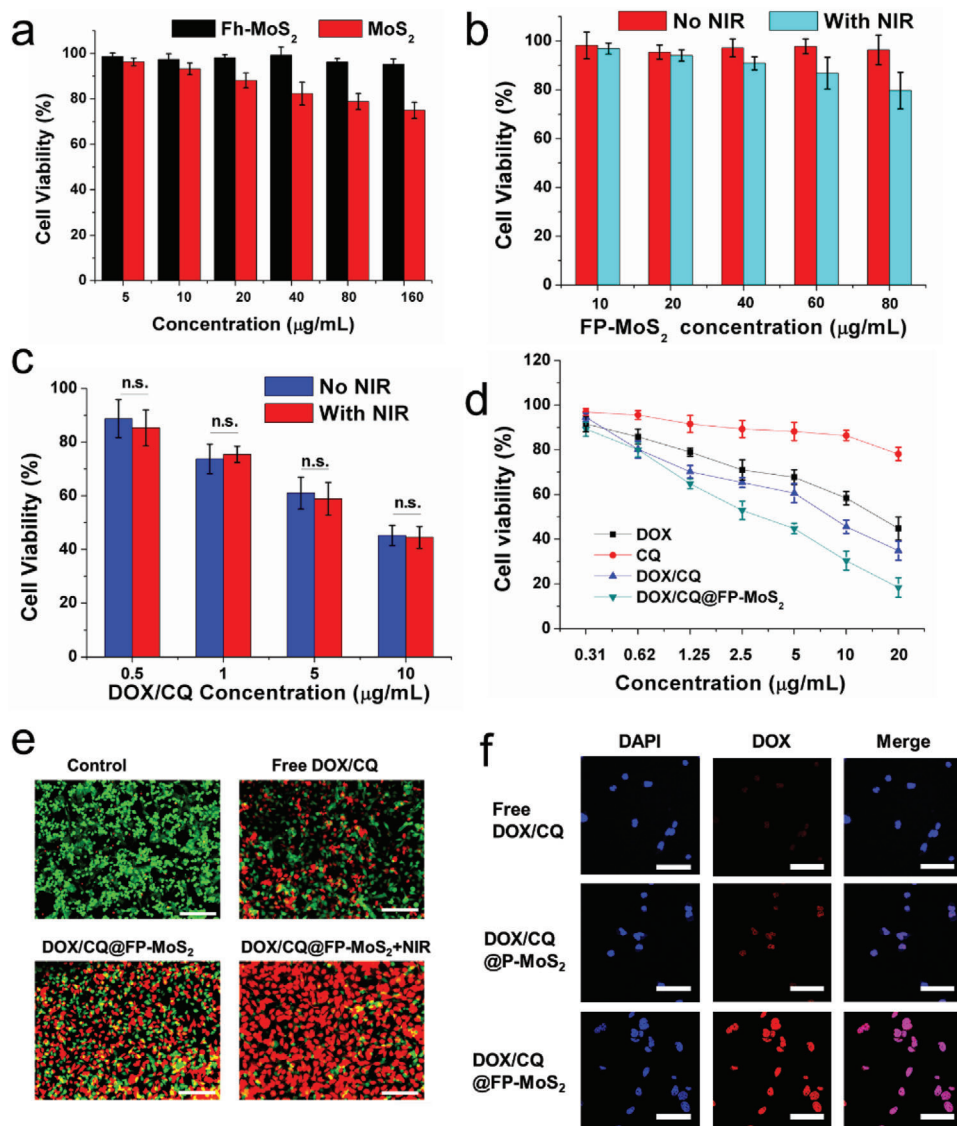


Figure 3. a) Cell viability of HeLa-R cells treated with MoS₂ and FP-MoS₂ for 48 h. Cell viability of HeLa-R cells exposed to b) FP-MoS₂ and c) free DOX/CQ (mass ratio = 1:1) for 48 h with or without NIR irradiation (NIR: 1 W cm⁻², 4 min). d) Cell viability of HeLa-R cells incubated with free DOX, free CQ, free DOX/CQ (mass ratio = 1:1), and DOX/CQ@FP-MoS₂ for 48 h. e) Fluorescence microscopy images of calcein-AM (green) and EthD-1 (red) co-stained HeLa-R cells after different treatments (scale bar, 200 μm). f) Confocal fluorescence images of HeLa-R cells after incubation with various materials. Red and blue colors represent DOX fluorescence and DAPI stained cell nuclei, respectively (scale bar, 50 μm). Concentrations of experimental groups in (e,f): free DOX/CQ (DOX at 5 $\mu\text{g mL}^{-1}$ and CQ at 5 $\mu\text{g mL}^{-1}$), DOX/CQ@P-MoS₂ (DOX at 5 $\mu\text{g mL}^{-1}$, CQ at 5 $\mu\text{g mL}^{-1}$, and P-MoS₂ at 40 $\mu\text{g mL}^{-1}$), DOX/CQ@FP-MoS₂ (DOX at 5 $\mu\text{g mL}^{-1}$, CQ at 5 $\mu\text{g mL}^{-1}$, and FP-MoS₂ at 40 $\mu\text{g mL}^{-1}$).

the future applications. The significantly enhanced antitumor efficacy, upon laser irradiation, was due to the photothermal triggered drug release from the nanosheets.

Intracellular localization of drugs, mediated by carrier, was also investigated by confocal laser scanning microscopy. As DOX destroy tumor cells by interaction with their DNA in the nucleus, the efficient delivery of DOX into the nuclei by carrier is necessary. According to confocal microscopy investigations, DOX uptake was increased after loading on FP-MoS₂ (Figure 3f). This effect was due to the existence of abundant folate receptors expressed on HeLa-R cells, which facilitated folic acid-mediated endocytosis of FP-MoS₂. These results demonstrated that the

modification of MoS₂ with folic acid facilitates the delivery of DOX into the HeLa-R cell nucleus, which can minimize the side effects of chemotherapy.

To gain more information about the antitumor activity of DOX/CQ@P-MoS₂ and to investigate the effect of targeting ligands conjugated to the sheets on their tumor penetration, multicellular tumor spheroids were established to mimic solid tumor tissue (Figure 4). Low fluorescence intensities were observed in the HeLa-R tumor spheroids treated with free DOX and DOX/CQ combinations, indicating limited penetration of the free drugs in tumor spheroids. Compared to DOX/CQ@P-MoS₂ treated group, which has no folic acid targeting ligands,

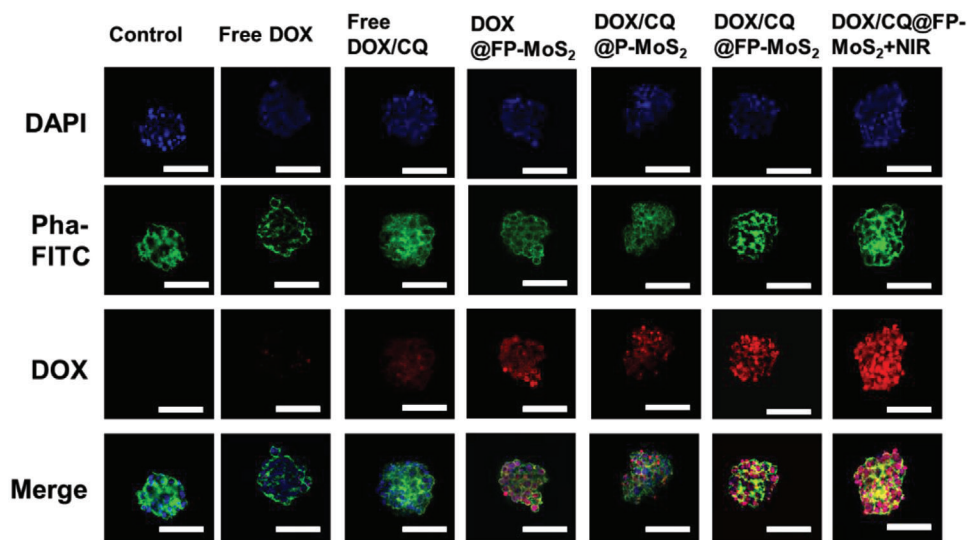


Figure 4. CLSM images of HeLa-R tumor spheroids incubated different samples. Blue, green, and red colors represent DAPI stained cell nuclei, Phalloidin FITC stained cell actin cytoskeleton and DOX fluorescence, respectively (scale bar, 100 μm). Concentrations of experimental groups were as follows: free DOX (DOX at 5 $\mu\text{g mL}^{-1}$), free DOX/CQ (DOX at 5 $\mu\text{g mL}^{-1}$ and CQ at 5 $\mu\text{g mL}^{-1}$), DOX@FP-MoS₂ (DOX at 5 $\mu\text{g mL}^{-1}$ and FP-MoS₂ at 40 $\mu\text{g mL}^{-1}$), DOX/CQ@P-MoS₂ (DOX at 5 $\mu\text{g mL}^{-1}$, CQ at 5 $\mu\text{g mL}^{-1}$, and P-MoS₂ at 40 $\mu\text{g mL}^{-1}$), DOX/CQ@FP-MoS₂ (DOX at 5 $\mu\text{g mL}^{-1}$, CQ at 5 $\mu\text{g mL}^{-1}$, and FP-MoS₂ at 40 $\mu\text{g mL}^{-1}$).

DOX/CQ@FP-MoS₂ treated group exhibited higher ability to transfer and accumulate DOX inside cells. And DOX@FP-MoS₂ treated group showed much stronger fluorescence than free DOX treated group, while not so strong as that of DOX/CQ@FP-MoS₂. Furthermore, we found that NIR irradiation further improved the penetration of DOX in tumor spheroids. Though the penetration of CQ is tough to track and visualize, but we can speculate that CQ may also be efficiently delivered into tumor tissue with the designed delivery carrier, owing to the similarities of DOX and CQ in physical and chemical properties.

3. Conclusion

The functionalization of MoS₂ nanosheets by polyglycerol improves their stability in aqueous solutions and results in poly-functional hybrid materials with the ability of loading and delivery a high amount of therapeutic agents. Moreover, bio-ligands such as folic acid can be conjugated to the polyglycerol coverage of nanosheets to target tumor cells. Triggering the release of cargos from the functionalized MoS₂ nanosheets amplify their therapeutic efficiency and result in the high anticancer effects, which was demonstrated for HeLa-R tumor spheroids.

4. Experimental Section

Materials: MoS₂ (powder, 99%), n-Butyllithium solution (n-BuLi, 2.5 M in hexane), N-Hydroxy succinimide (NHS), alpha-lipoic acid (LA), folic acid (FA), dimethyl sulfoxide (DMSO), dimethylformamide (DMF), 4'-6-diamidino-2-phenylindole (DAPI), chloroquine (CQ), dialysis bags (MWCO 2 kD), and phosphate-buffered saline (PBS) were purchased from Sigma-Aldrich.

Phalloidin FITC reagent was received from Abcam. Dialysis bags (MWCO 200 kD) was purchased from Spectrum Laboratories. Doxorubicin was obtained from abcr GmbH. CCK-8 and live/dead assay kits were

obtained from Thermo Fisher scientific. Multidrug-resistant HeLa cells (HeLa-R cells) and normal HeLa cells were provided by Leibniz Institute DSMZ (German Collection of Microorganisms and Cell Cultures). Hyper-branched polyglycerol (hPG) with $M_n \approx 10\,000\text{ g mol}^{-1}$ was synthesized according to reported procedure in literature.^[39] Milli-Q water was used in all experiments.

Methods: Zeta potential was measured by NANO ZSPO (Malvern) in water solution. Cell viability was investigated using a TECAN Infinite M200 Pro microplate reader with absorbance at 490 nm. Scanning electron microscopy (SEM) images were observed using Jeol JSM 7500F. Transmission electron microscopy (TEM) investigations were performed using Philips CM12 on a copper substrate. Thermogravimetric analysis (TGA) was performed on Linseis STA PT 1600 with a 10 $^{\circ}\text{C min}^{-1}$ heating rate under argon atmosphere. Nuclear magnetic resonance spectroscopy (NMR) spectra were recorded using Jeol Eclipse 600 MHz apparatus. Fourier transform infrared (FTIR) spectra were collected by a Thermo Fisher Nicolet 8700 spectrometer. UV-vis spectra were obtained by the UV-vis Spectrometer (Agilent Cary 8454). Confocal laser scanning microscopy (CLSM) images were taken by Leica TCS SP8 with 63 \times oil-immersion objective lens and processed by Leica confocal software. The laser irradiation was emitted by a diode infrared laser module (808 nm), Changchun New Industries, CN.

Preparation of MoS₂ Nanosheets: MoS₂ nanosheets were prepared by the lithium intercalation-exfoliation method according to the reported method in literature.^[40] Briefly, n-BuLi (2.5 M, 15 mL) in hexane was added to (0.5 g, 3.1 mmol) bulk MoS₂ and the mixture was stirred at 60 $^{\circ}\text{C}$ for 48 h under argon atmosphere. Then, the mixture was centrifuged, and the precipitate was collected. Then water was carefully added to the precipitates following by sonication for 4 h. Afterward, the aqueous suspension was centrifuged at 11 000 rpm for 1 h and the supernatant was discarded. The obtained black slurry was dispersed in water and dialyzed against water for 5 days to remove impurities.

Conjugation of Folic Acid and Lipoic Acid to hPG: Hyperbranched polyglycerol with 10% amino functional groups (hPG-NH₂-10%) was synthesized according to procedure in literature.^[41] In order to synthesize hPG with folic acid and lipoic acid functionalities (FA/LA-hPG), hPG-NH₂ (1 g, 0.1 mmol) was dissolved in DMF (10 mL). Lipoic acid (LA) (104 mg, 0.27 mmol), EDC (155 mg, 0.81 mmol) and NHS (12 mg, 0.1 mmol) were dissolved in DMF (5 mL) and added to the hPG-NH₂ solution. Afterward,

FA (119 mg, 0.27 mmol) was dissolved in DMSO (5 mL) and mixed with the above solution. The mixture was stirred at 40 °C for 24 h and dialyzed (dialysis bag MWCO: 2 kD) against CH₃OH/H₂O mixture for three days. Product was collected by lyophilization. hPG with only lipoic acid (LA-hPG) was synthesized using a similar approach.

Preparation of FA/LA-hPG Modified MoS₂ Nanosheets: FA/LA-hPG or LA-hPG (100 mg) was added into a water dispersion of MoS₂ nanosheets (400 mg in 20 mL water). After sonication for 1 h and stirring overnight, the solution was dialyzed with a dialysis bag (MWCO: 200 kD) to remove unconjugated polymer. The MoS₂ nanosheets with FA/LA-hPG and LA-hPG functionalities are abbreviated as FP-MoS₂ and P-MoS₂, respectively. Products were stored at 4 °C for further use.

Photothermal Effects: In order to evaluate the photothermal property of the functionalized MoS₂ nanosheets, different concentrations of FP-MoS₂ in PBS (pH 7.4) were irradiated by laser (808 nm). Different concentrations of FP-MoS₂ (50, 100, and 200 µg mL⁻¹) were irradiated for 4 min with 1.0 W cm⁻² power density. Also, FP-MoS₂ solution (200 µg mL⁻¹) was irradiated at various power densities (0.5, 0.75, and 1.0 W cm⁻²) over 4 min. As a control, the temperature change of PBS (pH 7.4) was also recorded. During NIR laser irradiation, the temperature was recorded at each time point and then the temperature changes were obtained compared with the initial medium temperature. Each experiment was repeated three times.

Loading and In Vitro Drug Release: FP-MoS₂ with the loaded DOX and CQ (DOX/CQ@FP-MoS₂) was prepared by mixing DOX (45 µg, 0.078 µmol), CQ (45 µg, 0.087 µmol) with 5 mL of FP-MoS₂ (20 µg mL⁻¹) aqueous dispersions. The mixture was stirred for 24 h at room temperature and pH 8.0. Then it was centrifuged at 4 °C and 10 000 rpm for 20 min. The precipitate was washed with water and centrifuged until no DOX and CQ were detected in the supernatant. The drug content in supernatants was measured, and the loading efficiencies were calculated to following formula: loading efficiency = $\frac{\text{total drug added} - \text{drug in the supernatants}}{\text{total drug added}} \times 100\%$. The obtained DOX/CQ@FP-MoS₂ was dispersed in water at 4 °C for the next experiments.

For the release studies, DOX/CQ@FP-MoS₂ dispersion was centrifuged and re-dispersed in PBS (pH 5.5 or pH 7.4) and shaken at 37 °C. At different time intervals (1 h, 2 h, 4 h, 8 h, 16 h, 28 h, and 40 h), 1 mL of the release media was taken out and replaced by 1 mL of fresh PBS. The excluded media was centrifuged and the drug content in the supernatant was measured by a microplate reader. For the NIR laser-triggered release, DOX/CQ@FP-MoS₂ dispersed in PBS (pH 5.5 and 7.4) was irradiated for 4 min by 1.0 W cm⁻² power density at certain time points (1 h, 2 h, 4 h, 8 h, 16 h, 28 h, and 40 h). Then 1 mL media was taken out and the released drug was measured as mentioned above.

In Vitro Cytotoxicity: The cytotoxicity of different materials against the HeLa-R cell line was evaluated using the CCK-8 assay. The resistance of HeLa-R cells to DOX was investigated using normal HeLa cells as a control.

For the biocompatibility test, HeLa-R cells were cultured in 96-well plates (5 × 10³ cells per well) overnight and then treated with different concentrations of pristine MoS₂ and FP-MoS₂ for 48 h. After incubation, the medium was removed, washed with PBS for three times and replaced with 100 µL of fresh medium containing 10 µL CCK-8. After additional 4 h incubation, 80 µL of medium was carefully taken out and its absorbance at 450 nm was determined. Cell viability was normalized by using the untreated cells as negative control.

The synergistic effects of DOX and CQ were also conducted. HeLa-R cells in 96-well plates were cultured overnight and they were treated with various concentrations of free DOX, free CQ and free DOX/CQ combinations (mass ratio at 4:1, 2:1, 1:1, 1:2 and 1:4) for 48 h. Then the medium was removed, washed with PBS and replaced with 100 µL of fresh medium and 10 µL CCK-8. After additional 4 h incubation, the absorbance (A) at 450 nm was measured to obtain the cell viabilities. The inhibition rate of each sample was calculated using the untreated cells as a control: Inhibition rate = $(A_{450\text{control}} - A_{450\text{sample}}) / A_{450\text{control}} \times 100\%$. Also IC₅₀ (half inhibitory concentration) values of DOX and CQ in all groups were calcu-

lated. The combination index (CI) of each group was calculated according to Chou and Talalay's method^[42-44]

$$CI = \frac{C(\text{DOX})}{IC_{50, \text{DOX}}} + \frac{C(\text{CQ})}{IC_{50, \text{CQ}}} \quad (1)$$

C(DOX) and C(CQ) represent the concentrations of DOX and CQ in the combination, respectively. IC_{50, DOX} and IC_{50, CQ} are the half inhibitory concentrations of DOX and CQ, respectively. The interactions of the two drugs can be categorized into synergistic (CI < 1), additive (CI = 1) and antagonistic (CI > 1) effects.

The NIR laser-induced cytotoxicity was measured in a similar method. After overnight incubation, the HeLa-R cells were treated with different concentrations of FP-MoS₂ and free DOX/CQ (mass ratio = 1:1). The experiment was duplicated as two groups. One group was subjected to NIR laser irradiation for 4 min (808 nm, 1 W cm⁻²) after incubation with different concentrations of FP-MoS₂ or free DOX/CQ for 6 h, and then additional 42 h. While the other non-irradiated group was incubated with the above-mentioned materials for 48 h directly. After incubation, the medium was removed, washed with PBS for three times and replaced with 100 µL of fresh medium containing 10 µL CCK-8. After additional 4 h incubation, 80 µL of medium was carefully taken out and its absorbance at 450 nm was determined. Cell viability was normalized by using the untreated cells as negative control.

For the in vitro antitumor evaluation, HeLa-R cells were cultured in 96-well plates (5 × 10³ cells per well) overnight and treated with various concentrations of free DOX, free CQ, free DOX/CQ (mass ratio = 1:1) and DOX/CQ@FP-MoS₂ for 48 h. The cytotoxicity of these vectors against the cells was evaluated as it was performed for the above-mentioned cytotoxicity testes.

In Vitro Live/Dead Assay: For the live/dead assay, HeLa-R cells were seeded in 12-well plates at a density of 1.5 × 10⁵ cells per well overnight. The cell medium was then replaced with fresh medium containing free DOX/CQ (mass ratio = 1:1) and DOX/CQ@FP-MoS₂ (DOX/CQ at the equivalent concentration of 5 µg mL⁻¹, MoS₂ at the concentration of 40 µg mL⁻¹). The DOX/CQ@FP-MoS₂ treated group was divided into two groups. One group was exposed to NIR irradiation for 4 min (808 nm, 1 W cm⁻²) in 6 h incubation time-frame and the other group was not irradiated. Cells without treatment were used as the negative control. After incubation for 24 h, the cells were washed with PBS for three times, followed by staining with calcein-AM (2 µM) and EthD-1 (4 µM) for 15 min. Finally, the cells were washed with PBS twice and observed under a fluorescence microscope (Zeiss Axio Observer Z1).

Intracellular Localization: HeLa-R cells were seeded on 8-well confocal laser Petri dishes at the density of 4 × 10⁴ cells per well and allowed to attach overnight. The culture medium was replaced with 300 µL of free DOX/CQ, DOX/CQ@P-MoS₂, and DOX/CQ@FP-MoS₂ (DOX/CQ at the equivalent concentration of 5 µg mL⁻¹, MoS₂ at the concentration of 40 µg mL⁻¹) respectively. After incubation in 6 h incubation time-frame and the other group was not irradiated, the cells were washed with PBS three times and fixed with 4% paraformaldehyde for 20 min. Then cells were washed three times with PBS and treated with 1% Triton-100 for 1 h. Subsequently, cells were washed three times with PBS and stained with DAPI for 30 min. The stained cells were observed with a confocal laser scanning microscope (Leica TCS SP8) at the excitation wavelength of 358 nm and 488 nm.

Tumor Spheroid Penetration: The spheroids of the HeLa-resistant cells were cultured for studying the penetration and distribution of the designed drug delivery system. HeLa cells were seeded in 24-well plates which precoated with poly(2-hydroxyethyl methacrylate) (pHEMA). All the cell culture medium for tumor spheroids was Dulbecco's Modified Eagle's Medium/Nutrient Mixture F-12 Ham containing 4 mg mL⁻¹ of bovine serum albumin. After 5 days, which spheroids grow to 100 µm diameter, the medium was replaced with fresh medium containing free DOX, free DOX/CQ, DOX/CQ@P-MoS₂, DOX/CQ@FP-MoS₂ (DOX/CQ at the equivalent concentration of 5 µg mL⁻¹, MoS₂ at the concentration of 40 µg mL⁻¹) and incubated with cells for 6 h. Cells without treatment were used

as control. Cells treated with DOX/CQ@FP-MoS₂ were divided into two groups. One group was exposed to NIR irradiation for 4 min (808 nm, 1 W cm⁻²) in 6 h incubation time-frame and the other group was not irradiated. Then the drug-containing medium was centrifuged, and the cells were washed with PBS three times. The cells were treated with 4%PFA, 0.1% Triton and 1% BSA respectively followed by incubation with DAPI/Phalloidin-FITC. Finally, the cells were washed with PBS and suspended in PBS for confocal imaging.

Supporting Information

Supporting Information is available from the Wiley Online Library or from the author.

Acknowledgements

S.X. gratefully acknowledges financial support from the China Scholarship Council. R.H. is grateful to the DFG for financial support. The authors acknowledge the core facility BioSupraMol, Cathleen Hudziak for hPG-NH₂ synthesis, and Dr. Pamela Winchester for polishing the language of this manuscript.

Open access funding enabled and organized by Projekt DEAL.

Conflict of Interest

The authors declare no conflict of interest.

Data Availability Statement

Research data are not shared.

Keywords

2D MoS₂, anticancer drug delivery, chloroquine, hyperbranched polyglycerol, multidrug-resistant cancer

Received: June 7, 2021
Revised: August 4, 2021
Published online: August 19, 2021

- [1] K. D. Miller, L. Nogueira, A. B. Mariotto, J. H. Rowland, K. R. Yabroff, C. M. Alfano, A. Jemal, J. L. Kramer, R. L. Siegel, *Ca-Cancer J. Clin.* **2019**, *69*, 363.
- [2] R. W. Robey, K. M. Pluchino, M. D. Hall, A. T. Fojo, S. E. Bates, M. M. Gottesman, *Nat. Rev. Cancer* **2018**, *18*, 452.
- [3] W. Ma, Q. Chen, W. Xu, M. Yu, Y. Yang, B. Zou, Y. S. Zhang, J. Ding, Z. Yu, *Nano Res.* **2021**, *14*, 846.
- [4] R. Ding, S. Jin, K. Pabon, K. W. Scotto, *Autophagy* **2016**, *12*, 737.
- [5] T. R. O'donovan, G. C. O'sullivan, S. L. McKenna, *Autophagy* **2011**, *7*, 509.
- [6] X. Zhang, X. Zeng, X. Liang, Y. Yang, X. Li, H. Chen, L. Huang, L. Mei, S. i-S. Feng, *Biomaterials* **2014**, *35*, 9144.
- [7] K. L. Bryant, C. A. Stalneck, D. Zeitouni, J. E. Klomp, S. Peng, A. P. Tikunov, V. Gunda, M. Pierobon, A. M. Waters, S. D. George, G. Tomar, B. Papke, G. A. Hobbs, L. Yan, T. K. Hayes, J. N. Diehl, G. D. Goode, N. V. Chaika, Y. Wang, G. - F. Zhang, A. K. Witkiewicz, E. S. Knudsen, E. F. Petricoin, P. K. Singh, J. M. Macdonald, N. L. Tran, C. A. Lyssiotis, H. Ying, A. C. Kimmelman, A. D. Cox, C. J. Der, *Nat. Med.* **2019**, *25*, 628.
- [8] M. Mauthe, I. Orhon, C. Rocchi, X. Zhou, M. Luhr, K. - J. Hijlkema, R. P. Coppes, N. Engedal, M. Mari, F. Reggiori, *Autophagy* **2018**, *14*, 1435.
- [9] D. Chen, J. Xie, R. Fiskesund, W. Dong, X. Liang, J. Lv, X. Jin, J. Liu, S. Mo, T. Zhang, *Nat. Commun.* **2018**, *9*, 873.
- [10] W. Zhou, H. Wang, Y. Yang, Z. - S. Chen, C. Zou, J. Zhang, *Drug Discovery Today* **2020**, *25*, 2012.
- [11] T. Kimura, Y. Takabatake, A. Takahashi, Y. Isaka, *Cancer Res.* **2013**, *73*, 3.
- [12] S. Ruan, R. Xie, L. Qin, M. Yu, W. Xiao, C. Hu, W. Yu, Z. Qian, L. Ouyang, Q. He, H. Gao, *Nano Lett.* **2019**, *19*, 8318.
- [13] J. - H. Sun, C. Ye, E. n-H. e Bai, L. - L. Zhang, S. - J. Huo, H. - H. Yu, S. u-Y. Xiang, S. - Q. Yu, *Nanotechnology* **2019**, *30*, 085101.
- [14] M. Vezmar, E. Georges, *Biochem. Pharmacol.* **1998**, *56*, 733.
- [15] H. Jin, C. Guo, X. Liu, J. Liu, A. Vasileff, Y. Jiao, Y. Zheng, S. - Z. Qiao, *Chem. Rev.* **2018**, *118*, 6337.
- [16] H. Zhang, *ACS Nano* **2015**, *9*, 9451.
- [17] Y. Song, Y. Luo, C. Zhu, H. e Li, D. Du, Y. Lin, *Biosens. Bioelectron.* **2016**, *76*, 195.
- [18] Y. Chen, Y. Wu, B. Sun, S. Liu, H. Liu, *Small* **2017**, *13*, 1603446.
- [19] X. Chen, J. - H. Ahn, *J. Mater. Chem. B* **2020**, *8*, 1082.
- [20] Z. Zhou, B. W. Li, C. Shen, D. Wu, H. C. Fan, J. Q. Zhao, H. Li, Z. Y. Zeng, Z. M. Luo, L. F. Ma, C. L. Tan, *Small* **2020**, *16*, 9.
- [21] T. Liu, Z. Liu, *Adv. Healthcare Mater.* **2018**, *7*, 1701158.
- [22] S. Sattari, S. Beyranvand, K. Soleimani, K. Rossoli, P. Salahi, I. S. Donskyi, A. Shams, W. E. S. Unger, A. Yari, G. Farjanikish, H. Nayebezhadeh, M. Adeli, *Langmuir* **2020**, *36*, 6706.
- [23] T. Liu, C. Wang, X. Gu, H. Gong, L. Cheng, X. Shi, L. Feng, B. Sun, Z. Liu, *Adv. Mater.* **2014**, *26*, 3433.
- [24] B. Huang, D. Wang, G. Wang, F. Zhang, L. Zhou, *J. Colloid Interface Sci.* **2017**, *508*, 214.
- [25] J. Shi, J. Li, Y. Wang, J. Cheng, C. Y. Zhang, *J. Mater. Chem. B* **2020**, *8*, 5793.
- [26] M. Caldera³N, M. A. Quadir, S. K. Sharma, R. Haag, *Adv. Mater.* **2010**, *22*, 190.
- [27] M. H. Staegemann, S. Gräfe, B. Gitter, K. Achazi, E. Quaas, R. Haag, A. Wiehe, *Biomacromolecules* **2018**, *19*, 222.
- [28] Z. Tu, H. Qiao, Y. Yan, G. Guday, W. Chen, M. Adeli, R. Haag, *Angew. Chem., Int. Ed.* **2018**, *130*, 11368.
- [29] I. S. Donskyi, Y. Chen, P. Nickl, G. Guday, H. Qiao, K. Achazi, A. Lippitz, W. E. S. Unger, C. Böttcher, W. Chen, M. Adeli, R. Haag, *Nanoscale* **2020**, *12*, 14222.
- [30] A. Faghani, I. S. Donskyi, M. Fardin Gholami, B. Ziem, A. Lippitz, W. E. S. Unger, C. Böttcher, J. P. Rabe, R. Haag, M. Adeli, *Angew. Chem., Int. Ed.* **2017**, *129*, 2719.
- [31] Z. Tu, I. S. Donskyi, H. Qiao, Z. Zhu, W. E. S. Unger, C. P. R. Hackenberger, W. Chen, M. Adeli, R. Haag, *Adv. Funct. Mater.* **2020**, *30*, 2000933.
- [32] S. Abbina, S. Vappala, P. Kumar, E. M. J. Siren, C. C. La, U. Abbasi, D. E. Brooks, J. N. Kizhakkedathu, *J. Mater. Chem. B* **2017**, *5*, 9249.
- [33] K. Wang, Q. Chen, W. Xue, S. Li, Z. Liu, *ACS Biomater. Sci. Eng.* **2017**, *3*, 2325.
- [34] X. Sun, R. Du, Li Zhang, G. Zhang, X. Zheng, J. Qian, X. Tian, J. Zhou, J. He, Y. Wang, Y. Wu, K. Zhong, D. Cai, D. Zou, Z. Wu, *ACS Nano* **2017**, *11*, 7049.
- [35] R. I. El-Gogary, N. Rubio, J. T.-W. Wang, W. T. Al-Jamal, M. Bourgoignon, H. Kafa, M. Naeem, R. Klippstein, V. Abbate, F. Leroux, S. Bals, G. Van Tendeloo, A. O. Kamel, G. A. S. Awad, N. D. Mortada, K. T. Al-Jamal, *ACS Nano* **2014**, *8*, 1384.
- [36] Z. Xu, X. Shi, M. Hou, P. Xue, Y. - E. Gao, S. Liu, Y. Kang, *Colloids Surf, B* **2017**, *150*, 50.
- [37] M. Wang, J. Li, X. Li, H. Mu, X. Zhang, Y. Shi, Y. Chu, A. Wang, Z. Wu, K. Sun, *J. Controlled Release* **2016**, *232*, 161.

- [38] Y. Qiao, J. Wan, L. Zhou, W. Ma, Y. Yang, W. Luo, Z. Yu, H. Wang, *Wiley Interdiscip. Rev.: Nanomed. Nanobiotechnol.* **2019**, *11*, 1527.
- [39] M. Wallert, C. Nie, P. Anilkumar, S. Abbina, S. Bhatia, K. Ludwig, J. N. Kizhakkedathu, R. Haag, S. Block, *Small* **2020**, *16*, 2004635.
- [40] E. E. Benson, H. Zhang, S. A. Schuman, S. U. Nanayakkara, N. D. Bronstein, S. Ferrere, J. L. Blackburn, E. M. Miller, *J. Am. Chem. Soc.* **2018**, *140*, 441.
- [41] J. I. Paez, V. Brunetti, M. C. Strumia, T. Becherer, T. Solomun, J. Miguel, C. F. Hermanns, M. Calderón, R. Haag, *J. Mater. Chem.* **2012**, *22*, 19488.
- [42] Z. Zhang, S. Xu, Y. Wang, Y. Yu, F. Li, H. Zhu, Y. Shen, S. Huang, S. Guo, *J. Colloid Interface Sci.* **2018**, *509*, 47.
- [43] T. - C. Chou, P. Talalay, *Adv. Enzyme Regul.* **1984**, *22*, 27.
- [44] T. - C. Chou, *Cancer Res.* **2010**, *70*, 440.